Oxygen-vacancy complexes in cerium oxide studied by ^{111}In time-differential perturbed-angular-correlation spectroscopy

Ruiping Wang and John A. Gardner
Department of Physics, Oregon State University, Corvallis, Oregon 97331-6507

William E. Evenson
Department of Physics and Astronomy, Brigham Young University, Provo, Utah 84602

James A. Sommers
Teledyne Wah Chang Albany, Albany, Oregon 97321
(Received 12 June 1992)

Four defect complexes with indium tracer atoms in undoped and lightly doped CeO_2 have been observed by ^{111}In time-differential perturbed-angular-correlation spectroscopy. One complex, identified as an indium–O-vacancy pair, is always present unless the material is doped with Nb or Ta to eliminate oxygen vacancies. The binding energy of the vacancy to indium is greater than 0.35 eV. In materials doped or annealed to introduce as little as 0.05% oxygen vacancies, two different double-vacancy complexes are formed. One is apparently a complex in which the vacancies are trapped on opposite sides of the indium along ⟨111⟩ directions. The other is likely a complex with one oxygen vacancy near the indium and one in a more distant trap. In material sufficiently doped with Nb, the majority of dilute indium dopants are uncomplexed, but a small fraction is strongly bound to a presently unidentified impurity. At low temperatures, an electronic excitation trapped at the time of the parent ^{111}In decay to ^{111}Cd clouds interpretation of some details. We speculate that this "aftereffect" affects only ^{111}Cd nuclei having no vacancies in their nearest-neighbor oxygen shell. Some complexes involving only more distantly trapped vacancies may be unobserved.

I. INTRODUCTION

Equilibrium ceria under standard temperature and pressure conditions has composition CeO_2 with a fluorite lattice. The material can be depleted easily of oxygen by annealing at elevated temperatures at reduced oxygen pressure. Lower valent dopants such as yttrium, several rare-earth elements, magnesium, and calcium also introduce free oxygen vacancies in ceria. The oxygen vacancies, which have an effective electrical charge +2, are energetically favored over electronic holes to compensate the dopant ionic charge. The vacancies have high mobility at elevated temperatures.[1]

Depending on composition, doping, and method of preparation, ceria and other group-IV oxides can have good electronic or, at elevated temperature, good oxygen ionic conductivity. They can also be made extremely tough; so they have great promise as structural and electronic ceramics. Because of their technological potential, the physical and electronic properties of the group-IV oxides have been extensively studied.[1,2] The fluorite phase of these oxides is of particular interest for electronic applications. The fluorite phase is stable at some temperature for most group-IV oxides and can usually be stabilized at room temperature by heavy alloying with group-II or -III elements. For undoped and lightly alloyed CeO_2, the fluorite phase is stable at all temperatures below the melting point.

We discuss in this paper a series of ^{111}In time-differential perturbed-angular-correlation (PAC) measurements on cerium oxide in which the concentration of oxygen lattice defects is controlled by doping and/or vacuum annealing at high temperatures. In all cases, the defect concentrations are dilute enough that the cerium oxide retains the fluorite structure. Indium is present only as an extremely dilute tracer, so its influence on bulk properties is negligible.

Some preliminary results of this investigation have been published previously.[3] We have also previously used ^{111}In PAC spectroscopy to study trapping and hopping of oxygen vacancies near indium and its daughter isotope, cadmium, in a variety of zirconia-based ceramics.[4–6] We have found indium-doped zirconia to be similar to zirconia doped with yttrium or trivalent rare-earth elements.

The work discussed in this paper shows that each indium probe atom in undoped and lightly doped ceria is strongly bound into a complex with axial symmetry. We identify the complex as a first-neighbor indium–oxygen-vacancy pair. PAC spectra at elevated temperatures indicate that the vacancy remains tightly bound to the indium and its ^{111}Cd daughter but that the vacancy can jump between equivalent near-neighbor positions over an activation barrier of 0.60(2) eV. This energy is equal to the diffusion barrier of free oxygen vacancies in cerium oxide.[7]

 ©1993 The American Physical Society

The vacancy-indium binding energy is greater than the binding energy of oxygen vacancies to yttrium or rare-earth dopants in ceria. The indium ionic radius is smaller than these other dopants. Scandium also has a small ionic radius and is known[1] also to have a large binding energy to oxygen vacancies in ceria.

When 0.05% or higher oxygen-vacancy concentrations are introduced by doping or high-temperature processing, the indium can trap another vacancy in one of two inequivalent structures. One of these structures is axial, leading to the hypothesis that two vacancies are trapped on opposite ($\langle 111 \rangle$ direction) corners of the surrounding first-neighbor oxygen cube. The second vacancy complex is nonaxial and is probably due to two trapped oxygen vacancies: one in a first-neighbor, and one in a second-neighbor position.

When ceria is doped with more than 400 ppm of Nb, most of the indium probe atoms are not associated with a structural defect. A small fraction, typically 5–25 % of the indium atoms, do form a strongly bound complex. The fraction of indium probe atoms that are complexed is not reproducible from sample to sample, and we suspect that these indium ions are bound to some low-concentration unintentional impurity.

II. ^{111}IN PAC METHOD AND PROCEDURE

The experiments described here require samples in which radioactive ^{111}In is present. The ^{111}In decays by electron capture, half-life 2.8 days, to an excited state of ^{111}Cd which then decays to its ground state by successive emission of 171- and 245-keV γ rays through an intermediate state with half-life 85 ns. If the nucleus is unperturbed, there is a substantial angular anisotropy, characterized by the parameter A_2, between the emission directions of the two γ rays. The angular anisotropy depends on the time between the two γ ray emissions if the nucleus is subject to perturbing fields. Measurement of this time-dependent perturbation in order to find the perturbing fields is the object of a PAC experiment.

A total activity of order 10^4–10^5 disintegrations and an accumulation time of 12–24 h is required for a typical measurement; so about a dozen measurements can be carried out before a well-made sample becomes too weak. All our samples, whose synthesis is discussed in the next section, were random polycrystalline powders, and our discussion is confined to this special case.

Our PAC spectrometer has four BaF_2 scintillation detectors in a plane at mutual 90° angles.[8] Samples are heated by a thin-walled water-cooled furnace capable of temperatures up to 1400°C. The controlling microcomputer collects histograms of events in which the first γ ray of the ^{111}Cd nuclear decay enters detector α and the second γ ray enters detector β at time t later. In the Appendix we describe the procedure for combining these histograms to obtain the experimental time function $A_2G_2(t)$ which provides all physical information available from these PAC measurements. Here A_2 is the effective anisotropy, typically -0.10 to -0.15 in our experimental geometry. The perturbation function $G_2(t)$ should be unity if the ^{111}Cd nucleus is unperturbed during the time between emission of the two γ rays. $G_2(t)$ is a well-understood oscillatory function if the nucleus is subject to a static magnetic and/or electrostatic interaction.[9] We confine our discussion to electric quadrupole interactions, since magnetic interactions are negligible for the material of interest here.

When all nuclei in a sample are subject to an interaction between the ^{111}Cd nuclear quadrupole moment and a static electric field gradient (EFG), $G_2(t)$ is given by

$$G_2(t) = S_0 + \sum_{i=1}^{3} S_i \cos \omega_i t, \tag{1}$$

where ω_1, ω_2, and $\omega_3 = \omega_1 + \omega_2$ are, respectively, the smaller, larger, and sum of the frequency splittings of the ^{111}Cd ($I = \frac{5}{2}$) intermediate nuclear state subject to an EFG. The EFG is normally characterized by a magnitude V_{zz} and asymmetry η.[9] The weighting factors S_i depend on η; ω_1 depends on η and is proportional to V_{zz}. The

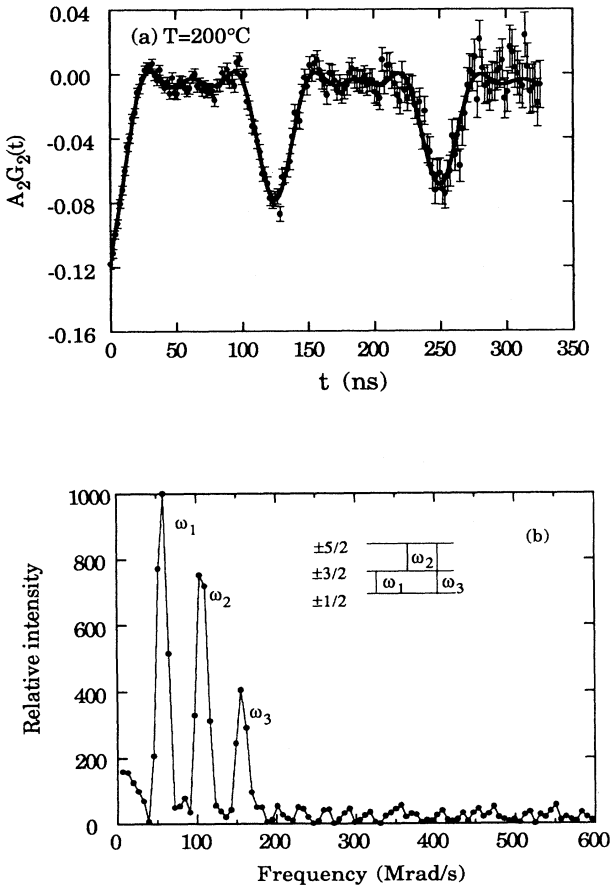

FIG. 1. (a) PAC time function and (b) Fourier transform for trace concentration ^{111}In in cerium oxide at 200°C. The sample was cooled slowly in air after synthesis and was exposed to air during measurement. The inset in (b) shows the relationship between the observed frequencies and the ^{111}Cd intermediate state energy levels in an electric field gradient. Solid lines are the computer fit discussed in the text for site A.

ratio ω_2/ω_1 is a monotonic function of η that falls from 2 to 1 as η varies from 0 (axially symmetric EFG) to 1 (maximally asymmetric EFG).

A typical experimental time function for an undoped cerium oxide host is shown in Fig. 1. The Fourier transform clearly shows the three frequencies. The physical origin of the frequencies is illustrated by the inset which shows the nuclear level diagram for the intermediate ^{111}Cd state subject to a static EFG interaction. For the data of Fig. 1, $\omega_2/\omega_1 = 2$, indicating an axial EFG. As discussed below, careful analysis of the data shown in Fig. 1 indicate that the EFG is not entirely static, but at this temperature the EFG time dependence is barely detectable.

In general, all nuclei in a sample are not subject to the same interaction. Minor variations in EFG's due to dilute impurities or structural defects are usually approximated by assuming a distribution for V_{zz}. There may be a number of inequivalent sites occupied by PAC probe atoms. If the fractional occupation probability of a site j is f_j and the perturbation function appropriate to the site is $G_2^j(t)$, then the measured time function is

$$G_2(t) = \sum_j f_j G_2^j(t) \,. \tag{2}$$

Most of the interactions studied in this paper are due to defect complexes of the indium probe atom with oxygen lattice defects. At elevated temperature, oxygen atomic diffusion times can be nanoseconds or less, and the EFG can fluctuate on this time scale. Models appropriate for such experiments have been studied in detail,[10,11] and we make extensive use of these model results for data analysis.

We note that ^{111}In PAC detects interactions with the daughter ^{111}Cd nucleus, not the parent ^{111}In. At low temperature, the lattice defect responsible for a particular interaction is trapped by the indium parent, but there may be a substantial local lattice relaxation following transmutation to cadmium. The first γ ray of the ^{111}Cd cascade is emitted within a few nanoseconds after ^{111}In decays by capturing an inner-shell electron. This time is sufficient for the lattice to relax about the cadmium but, in poorly conducting materials, may be too short to permit the electronic state population to reach equilibrium. A Cd dopant in ceria is likely to have deep acceptor levels. If holes are trapped in these levels after the ^{111}In decay, a strong and poorly understood interaction between the hole and the ^{111}Cd nucleus causes a rapid decay of $G_2(t)$. Such "aftereffects" associated with the initial electron capture decay are common for ^{111}In PAC measurements on insulators.[12,13]

III. SAMPLE PREPARATION

All samples were made by precipitation from a cerium ammonium nitrate $[(NH_4)_2Ce(NO_3)_6]$ stock solution to which a few drops of the ^{111}In radioactive tracer were added prior to precipitation. The ^{111}In was purchased from the New England Nuclear division of Dupont as a HCl solution. The concentration of ^{111}In is of order 10^{-9}/(formula wt.) for a typical sample of mass of about 100 mg and having an activity of a few μCi when freshly prepared. To make samples doped with Y, an appropriate amount of yttrium nitrate solution was first added to the stock solution and well mixed. Nb dopants were incorporated by adding an oxalic acid solution of niobium hydrous oxide. One Ta-doped sample was made by adding a sulfuric acid solution of $TaCl_5$. The Ta solution with the cerium ammonium nitrate is unstable, and the two solutions were mixed immediately prior to making the sample. Other mixtures appear to be stable over a period of many months.

After extensive stirring to mix all components, samples were precipitated by adding a concentrated ammonium hydroxide solution while stirring vigorously. The cerium hydrous oxide precipitate was filtered, washed carefully and then dried until most of the water had evaporated, leaving a loose fine powder. The powder was then placed in an aluminum oxide sample holder and calcined (heated in air) to convert the material to (doped) cerium oxide.

Cerium ammonium nitrate solutions used for most samples were purchased from J. T. Baker. These solutions contain cation impurities, largely rare-earth metals, at a level of approximately 300 ppm total. In order to reduce the impurity concentration, a second cerium ammonium nitrate stock solution was made by dissolving high-purity cerium oxide, obtained from the Ames Rare Earth Research Laboratory. The starting material and final stock solution contained cation impurities at a level of approximately 10 ppm total. Undoped samples made from the first solution were pale yellow, whereas samples from the second solution were white, but PAC spectra were indistinguishable.

Initial PAC data were accumulated for samples that had been calcined at 1000°C. Figure 2(a) shows the $A_2G_2(t)$ spectrum of such a sample collected at 800°C. The majority of indium atoms clearly sit in a cubic environment (zero EFG) with negligible damping, as expected for substitutional dopants in a site of cubic symmetry. However, a substantial fraction of indium probes show a rapid reduction of anisotropy near the origin, as seen in Fig. 2(a). We attribute this spectral feature to nuclei in grain boundaries, amorphous regions, or other material that is not representative of the bulk crystal. Such environments subject probe nuclei to interactions with a wide frequency distribution. Samples calcined at 1600°C for 6 h produced the 800°C spectrum of Fig. 2(b). For this case, $G_2(t)$ is unperturbed, indicating that all indium atoms are dissolved in the bulk, that the time-average interaction is zero, and that damping is negligible. Electron micrographs of samples calcined at 1000°C and 1600°C indicate submicrometer grain sizes for the first and of order 10 μm for the latter. Later measurements have indicated that calcining at 1200°C is sufficient to dissolve all indium, but all data reported here were taken with samples calcined at 1550–1600°C for 6 h and cooled to room temperature in approximately 2 h.

Indium oxide is volatile at calcining temperatures, and we typically found that samples lost 25–50 % of their indium activity during calcination at 1550–1600°C. The indium that evaporated from the cerium oxide was partly

absorbed by the aluminum oxide sample holder and partly deposited on the seals and baffles of the calcining furnace. Before transferring to the PAC spectrometer, the cerium oxide was placed in a clean sample container. The container was usually an alumina cylinder having outside diameter 5 mm and 1 mm wall thickness, but zirconia and platinum containers were used on occasion to check for possible sample-holder contamination. No evidence was found that any indium was lost from the cerium oxide during PAC data accumulation, even at temperatures as high as 1000°C.

The dopant concentrations of Y-, Nb-, or Ta-doped samples given here are nominal concentrations. Chemical analysis of a few representative samples with larger doping levels agrees well with the nominal compositions.

We attempted to make samples doped with 0.1–1.0 at.% (nonradioactive) indium to compare with Y-doped materials, but a great deal of the indium evaporated during calcination. Subsequent chemical analysis showed that the indium concentration was comparable to or smaller than that of unintentional impurities. PAC spectra on such samples were indistinguishable from those of undoped ceria.

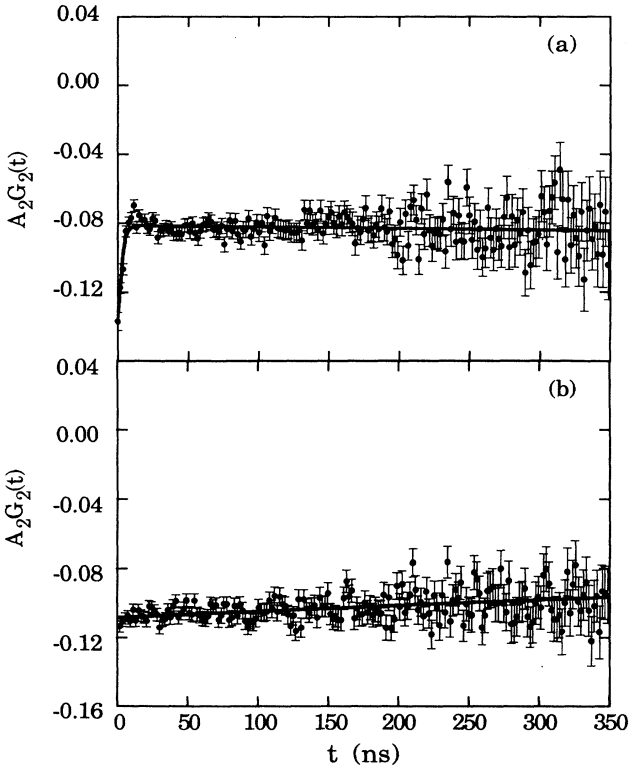

FIG. 2. PAC time functions for trace concentration ^{111}In in two undoped ceria samples at 800°C. Both were exposed to air during measurement. Sample (a) was calcined at 1000°C and had submicrometer grains. Sample (b) was calcined at 1600°C and had grains of order 10 μm. The rapid $G_2(t)$ decay near the origin in (a) is attributed to ^{111}In nuclei in regions not representative of the bulk crystal. In sample (b) all ^{111}In is dissolved in the bulk.

IV. EXPERIMENTAL RESULTS

A. Undoped cerium oxide

Figure 3 shows the experimental time function for undoped cerium oxide in air at a number of temperatures. Below 300°C, the time function has a well-defined oscillation indicating that a large fraction of the Cd nuclei are in an environment, denoted site A, where they are perturbed by an EFG. The frequency triplet of this interaction is illustrated clearly in Fig. 1(b).

Below 150°C, a substantial fraction of PAC nuclei are subject to a strong damping that is characteristic of the nuclear decay "aftereffects." We refer to this interaction as site X. The fraction of nuclei in site X is approximately 55% near and below room temperature but becomes negligible for T above 150°C.

Near and above 300°C the PAC time functions indicate that the Cd nucleus is subject to a time-dependent EFG. Above 300°C the EFG time average is zero, but the fluctuation rate is slow enough to cause damping of the anisotropy. The damping rate decreases with temperature, becoming negligible above 800°C where the time function $A_2G_2(t)$ is unperturbed and has the full expected anisotropy.

We show later that these data are consistent with a model in which the EFG is constant in magnitude but reorients at a rate w that increases with temperature. Figure 4 shows the interaction frequencies ω_1 and ω_2 vs temperature. The reorientation rate is shown in Fig. 5.

Figure 6 shows the PAC time function for undoped ceria that has been depleted of oxygen by annealing for 30 min in reduced oxygen pressure at 1200°C and sealed. The data are qualitatively similar to those of ceria held in air but have more complicated oscillatory behavior at low temperature. Fourier transforms of the 200°C data are shown in Fig. 7.

In addition to the frequency triplet (A) shown in Fig. 1, the more strongly oxygen-depleted samples have the two frequency triplets indicated by B and C in Fig. 7. The frequencies of nuclei subject to the B and C site interactions are shown in Fig. 4. The fractions f_A, f_B, and f_C of the three sites at 200°C are shown vs estimated oxygen deficiency c in Fig. 8.

The reorientation rate for the B site is shown in Fig. 5. The C-site EFG is also time dependent. Its fluctuation rate must be roughly the same as that of A and B, but it cannot be determined with confidence.

B. Nb- and Ta-doped ceria

Figure 9 shows the experimental PAC time function at several temperatures for a sample doped with 500 ppm Nb/(formula wt.) in order to introduce an excess of positively charged dopants. Figure 9 is representative of spectra for samples containing at least 400 ppm Nb/(formula wt.). Spectra of all samples doped with 300 ppm or less Nb are indistinguishable from those for undoped cerium oxide. No substantial difference is observed between samples made from the low- and high-purity starting cerium solutions. For Nb doping between 300 and 400 ppm, the

PAC spectra were generally a superposition of the two different kinds of spectrum. Unfortunately, the accuracy and homogeneity of doping was not reproducible enough to allow the transition to be characterized clearly.

The time functions shown in Fig. 9 display a time-dependent decay modulated by a small amplitude oscillation. Analysis of these data indicate that most ^{111}In probe nuclei are in uncomplexed substitutional sites but that a small fraction are strongly bound into a complex unrelated to the bound vacancies discussed above.

We attribute the amplitude decay of $G_2(t)$ to the aftereffects interaction discussed in Sec. II. We show in the Appendix that these data permit determination of the escape rate r of the electronic disturbance responsible for the aftereffects. r is shown in Fig. 10.

The small oscillations in the data of Fig. 9 are due to a static EFG interacting with a small fraction of the ^{111}Cd nuclei. These (site D) interaction frequencies are shown in Fig. 4. The frequencies are reproducible, but the fractions vary from sample to sample. The fraction is generally between 5 and 25%. It decreases as T increases and becomes small for large Nb concentration.

PAC data similar to those shown in Fig. 9 were found for ceria doped with 500-ppm Ta, indicating that the change from undoped ceria behavior is caused by pentavalent doping, not by some interaction specific to Nb.

One 500-ppm Nb-doped sample was annealed at 1200°C and 30 mTorr O_2 pressure and sealed in a fused silica capsule before being cooled to room temperature. The sample was then opened to air and PAC measurements were made at room temperature, 100, 200, and 300°C. The first three data sets were similar to those of the O-depleted sealed undoped ceria samples described above. At 300°C, the data reverted to a PAC time function like that of Fig. 9. These results indicate clearly that this sample was oxygen deficient after being quenched

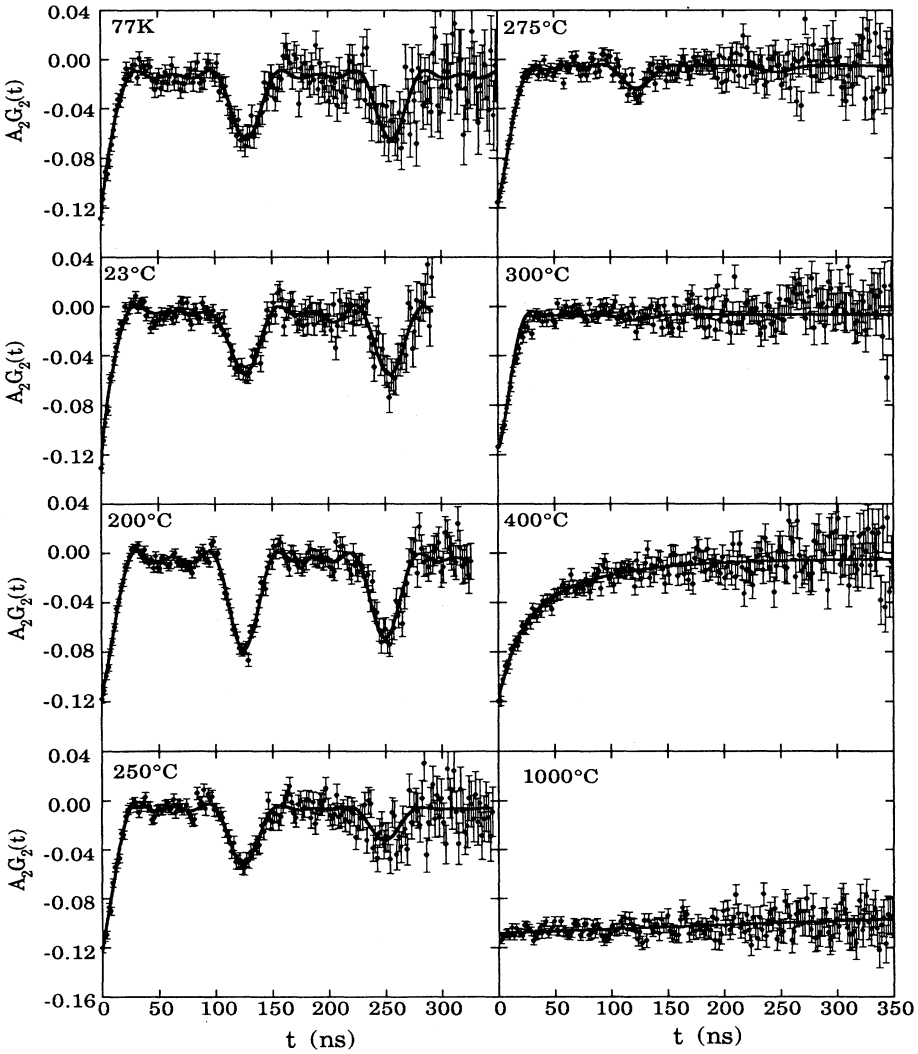

FIG. 3. PAC time functions for trace concentration ^{111}In in undoped ceria held in air at the temperatures indicated, except at 77 K where the sample was immersed in liquid nitrogen. Solid lines are computer fits discussed in the text.

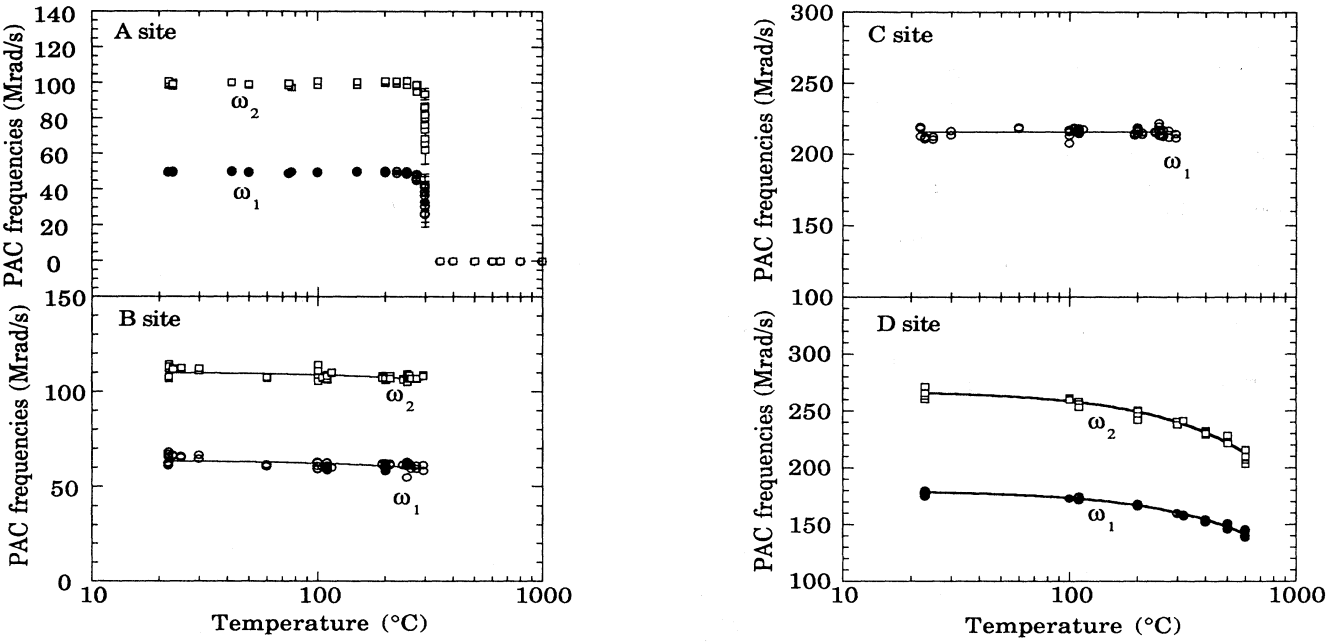

FIG. 4. Interaction frequencies for the A, B, C, and D sites. These sites and the fitting procedures are described in the text.

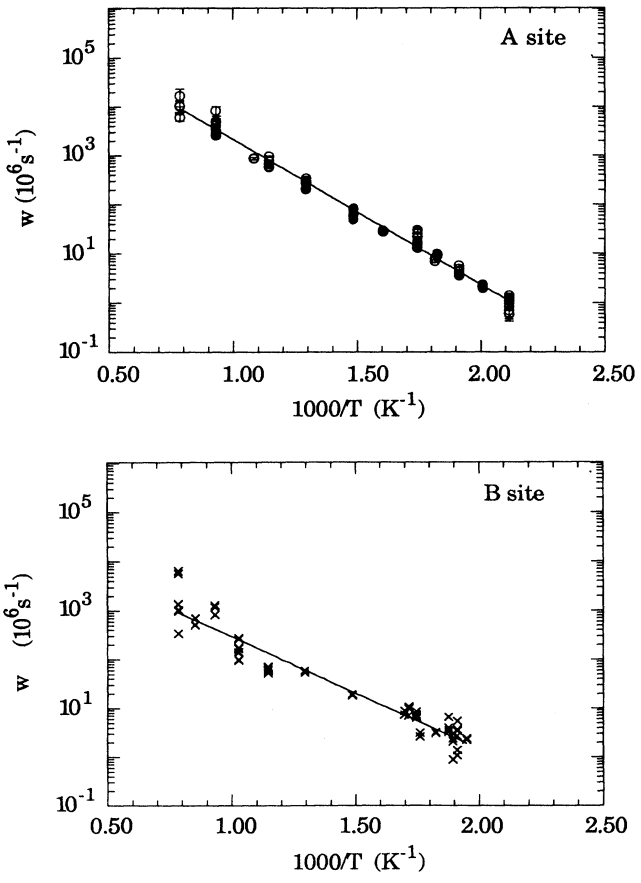

FIG. 5. Fluctuation rate w for EFG reorientation for A and B sites.

and that equilibrium was reestablished between 200 and 300°C.

C. Y-doped ceria

PAC data for ceria doped with yttrium up to 0.1% (formula wt.) are indistinguishable from those of undoped ceria. For larger yttrium doping levels, the data are qualitatively similar to those of oxygen-depleted ceria shown in Fig. 6. The same frequency triplets arising from EFG interactions at A, B, and C sites are seen. The fractions of these three sites at 200°C in Y-doped and oxygen-depleted undoped ceria are shown in Fig. 8.

V. DISCUSSION OF EXPERIMENTAL RESULTS

A. Oxygen-vacancy concentration, c

Oxygen vacancies play a critical role in these experiments, and we consider here the factors that control the vacancy concentration. For samples slowly cooled in air and measured below 500°C, the density of thermally generated lattice defects should be negligible. Deviation from the ideal CeO_2 stoichiometry for these samples should be determined largely by impurities whose electrical charge is compensated by excess oxygen vacancies or interstitials.[1] Impurities in our cerium solutions could lead to a total oxygen vacancy concentration, c, of order 75–100 ppm in our normal quality undoped samples or about 5 ppm in our highest-purity undoped ceria samples.

Samples doped with the pentavalent metals, Nb or Ta, are expected to have an excess concentration of nega-

tively charged oxygen interstitials or interstitialcies to compensate the excess positive charge of the pentavalent impurities. We have introduced Nb, and in one case Ta, primarily to compensate the charge of unintentional lower-valent dopants and consequently to reduce the oxygen-vacancy concentration c. For sufficiently large pentavalent doping levels, c should become negligible.

Yttrium impurities, which have an effective charge of -1, introduce oxygen vacancies (effective charge $+2$). If other impurities are negligible, a concentration x per formula wt. of yttrium dopants should introduce an oxygen-vacancy concentration $c = x/4$. In general, some fraction of these vacancies will be bound to lower-valent impurities.[1,7] If one assumes that the free oxygen vacancies can be trapped by an impurity in one of N equivalent sites, with energy $-E_b$, or may be free, with energy zero, then the fraction f of any impurity species with a bound vacancy at temperature T (fictive temperature for quenched samples) is

$$f = \frac{Ne^{(\mu+E_b)/kT}}{1+Ne^{(\mu+E_b)/kT}} . \tag{3}$$

For small free oxygen-vacancy concentration c_{fv}, the chemical potential μ is given by

$$c_{\mathrm{fv}} = e^{\mu/kT} . \tag{4}$$

Then

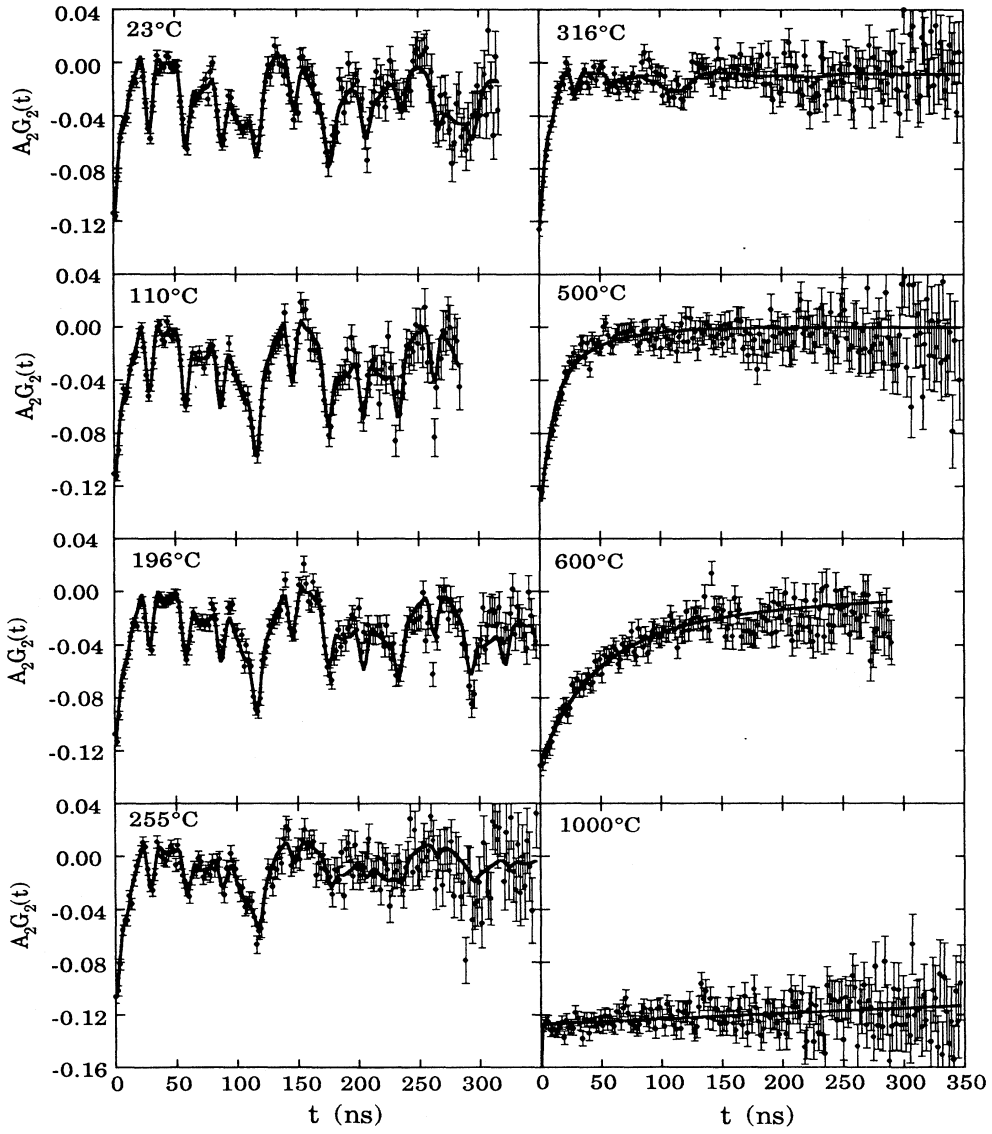

FIG. 6. PAC time functions at temperatures indicated, for trace concentration ^{111}In in undoped ceria sealed in fused silica capsules after being depleted of oxygen by annealing for 30 min at 1200°C and p_{O_2} pressure 5 mTorr. The estimated oxygen loss c is 0.25%.

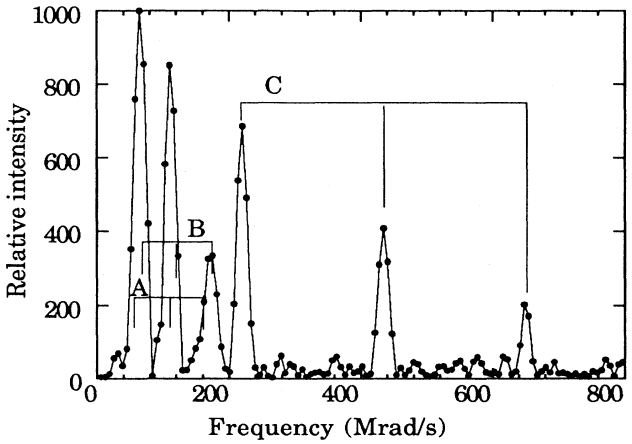

FIG. 7. Fourier transform of 200°C data of Fig. 6 showing existence of sites A, B, and C.

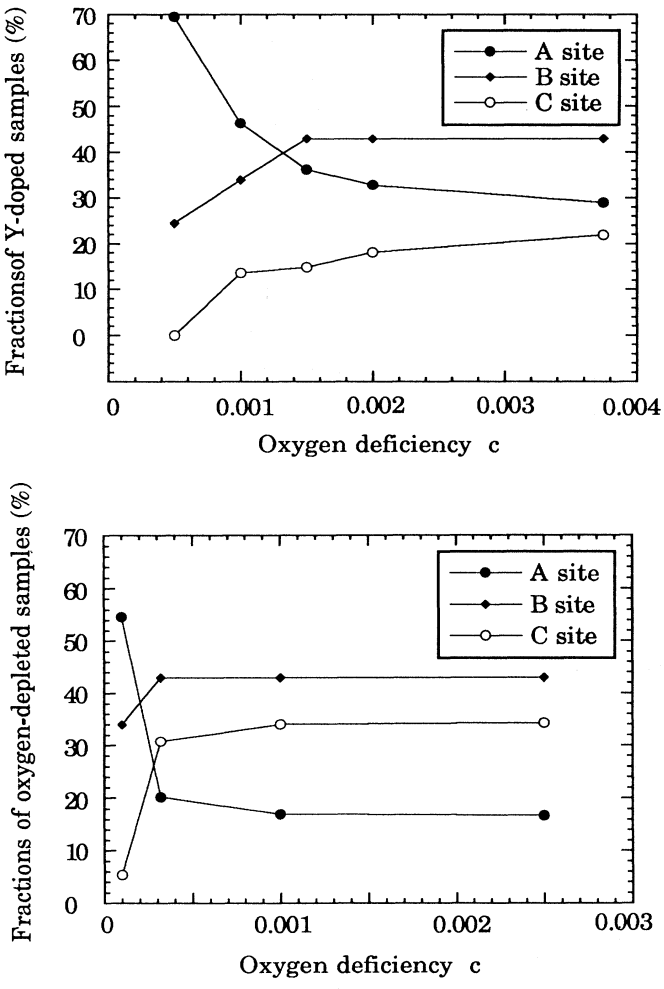

FIG. 8. Fractions of nuclei in A, B, and C sites, respectively, vs oxygen deficiency c at 200°C. For oxygen-depleted samples of $CeO_{2(1-c)}$, c is estimated from preparation conditions. For Y-doped samples of $Ce_{1-x}Y_xO_{2(1-c)}$, charge balance requires that $c = x/4$.

$$f = \frac{1}{1 + e^{-E_b/kT}/Nc_{\mathrm{fv}}} . \tag{5}$$

The binding energy of oxygen vacancies to yttrium is about 0.3 eV.[7] At 200°C most vacancies should be free for yttrium concentrations of order 0.1% or less, but a substantial fraction should be bound to Y atoms for the larger Y-doping levels used in this work.

At elevated temperatures, ceria becomes significantly depleted of oxygen.[14] In this case the positive charge of the oxygen vacancies is compensated by conduction electrons. There is a substantial binding energy between the vacancies and electrons,[15,16] so when these oxygen-depleted samples are quenched, there will, in general, be a substantial number of singly charged vacancies as well as simple (doubly positive-charged) vacancies and free electrons. The oxygen-vacancy concentration given in Fig. 8 is computed from the data of Ref. 14 without regard to the charge.

B. Site *A*

For undoped and lightly doped ceria samples that have not been deliberately depleted of oxygen, the PAC Fourier transform spectrum at 200°C has a single triplet with frequencies accurately in the ratio 1:2:3 characteristic of an axially symmetric electric field gradient interaction. We have referred to this as site A. It is also found in the PAC spectra of oxygen-depleted quenched undoped ceria and in Y-doped ceria but not in samples doped with more than 300 ppm of Nb. At lower temperatures some fraction of the ^{111}Cd nuclei are subject to aftereffects, but we defer discussion of aftereffects-related phenomena to a later section.

Computer fits to the time function $G_2(t)$ give the frequencies shown in Fig. 4 for site A. The site-A frequencies are very sharp below 200°C but become broader at higher temperatures. The temperature dependence of the series of $G_2(t)$ functions indicates clearly that the broadening is due to the time dependence of the EFG on the PAC time scale. The $G_2(t)$ are very well fitted at all temperatures by a simple fluctuating EFG model described in the Appendix and Refs. 10 and 11. The model assumes an axially symmetric EFG whose symmetry axis can fluctuate among three mutually perpendicular orientations at rate w. This model should be appropriate for a strongly bound vacancy that can hop among a number of equivalent positions or for any other axial complex that can reorient randomly with time. We assume implicitly that all indium atoms and their cadmium daughters remain bound in this complex at all temperatures. If significant dissociation occurs at elevated temperature, the model could still provide reasonable fits to the experimental time function, but the fitted value of w would be incorrect. In such circumstances the fitted w values at high temperature would not follow the activated behavior extrapolated from low temperature. All w values shown in Fig. 5 agree well with a single activation energy of 0.60(2) eV, and we take this as evidence that no substantial dissociation occurs below 700°C. At higher

temperature, fitting errors are too large to draw firm conclusions.

The plausible explanation for these observations is that an oxygen vacancy is strongly bound to each indium atom and that the vacancy can jump among trap sites over an activation barrier of 0.60(2) eV. This energy is the same as the free vacancy jump barrier of 0.6 eV deduced from ionic conductivity experiments.[7] In principle, the indium-vacancy pair binding energy can be determined from the concentration dependence and temperature dependence of the pair probability. If the binding energy were comparable to that of most trivalent dopants (about 0.1–0.3 eV), the A-site fraction at a given temperature should vary smoothly, increasing with Y doping and decreasing with Nb doping. We find, however, that the fraction changes abruptly from unity to zero as the Nb-doping concentration is changed from 300 to 400 ppm/(formula wt.). Our interpretation of this observation is that our undoped material contains approximately 75 ppm of oxygen vacancies which require 300 ppm Nb to remove and that the binding energy of vacancies to indium is more than 0.35 eV. The homogeneity and accuracy of Nb doping cannot be controlled well enough to determine anything other than a lower bound of approximately 0.35 eV for E_b.

An oxygen-vacancy concentration of 75 ppm is much larger than expected for our best samples. Although we took care to keep contamination to a minimum, it is possible that aluminum was introduced during processing, since most samples were synthesized in alumina labware in an alumina-lined furnace. Chemical analysis of samples shows some aluminum contamination but cannot de-

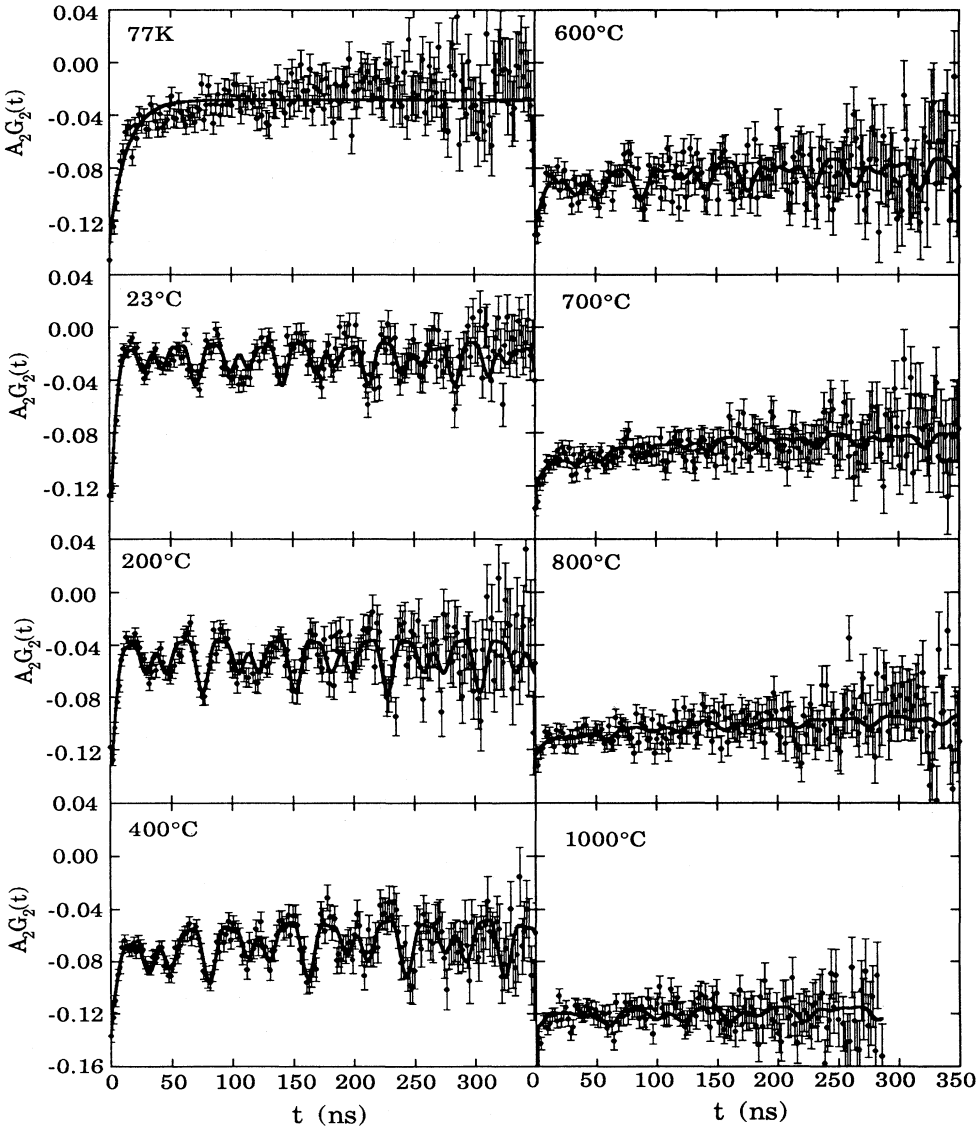

FIG. 9. PAC time functions for trace concentration ^{111}In in cerium oxide doped with 500 ppm Nb/(formula wt.). Samples were held in air at the indicated temperatures except at 77 K where they were immersed in liquid nitrogen.

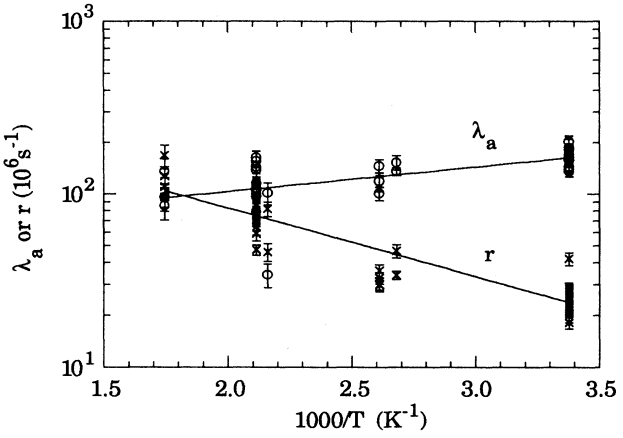

FIG. 10. Decay rate λ_a and hole escape rate r vs temperature for nuclei in Nb-doped samples.

termine whether the aluminum is dissolved in the ceria or is present as small alumina flakes from labware or furnace wall flakeoff. Alumina flakes would not affect PAC data. Unfortunately, we have no alumina-free processing facilities and have not yet been able to determine whether dissolved aluminum is responsible for the unexpectedly large oxygen-vacancy concentration of otherwise undoped ceria.

We have used a simple point ion model to compute the EFG caused by a vacancy in an unrelaxed lattice. The computed value for a second-neighbor vacancy is approximately equal to that of site A, whereas the EFG computed for a first-neighbor vacancy is almost a factor of 4 larger. The point-ion approximation is reasonable for this material, but our neglect of lattice relaxation is not. In particular, any lattice relaxation around a second-neighbor vacancy should cause the complex to be nonaxial. Lattice relaxation around a first-neighbor vacancy would preserve axial symmetry but could alter the EFG magnitude significantly. It is possible that the site-A EFG is due to a trapped second-neighbor vacancy and that the asymmetry is too small to be observed or that the EFG is due to a first-neighbor vacancy and that the EFG magnitude is reduced because of local lattice relaxation. We believe that the latter hypothesis is the more reasonable one. The hypothesis can be tested definitively by single-crystal PAC measurements which can distinguish clearly between field gradients with symmetry axes along $\langle 111 \rangle$ (first-neighbor) as opposed to $\langle 311 \rangle$ (second-neighbor) directions. Such experiments are planned.

C. Sites B and C

These sites are found only when c exceeds a few hundred ppm, so they can only be complexes of indium dopants with more than one trapped vacancy. The C site has axial symmetry; so it can only be a complex with vacancies trapped at positions $\mathbf{r}$ and $-\mathbf{r}$ with respect to the PAC probe atom. Point-ion unrelaxed-lattice calculation of the EFG for such a linear complex with the vacancies in first-neighbor ($\langle 111 \rangle$) positions gives an EFG magnitude that is twice the observed value. The same kind of calculation for vacancies in second-neighbor ($\langle 311 \rangle$) positions gives a value half that observed. We believe that the most reasonable hypothesis for the C complex is that the trapped vacancies are at ($\langle 111 \rangle$) near-neighbor sites and that the remaining six oxygen neighbors to the PAC probe relax to reduce the EFG magnitude below the value calculated for an unrelaxed shell. This is consistent with the A-site hypothesis and can also be tested by single-crystal PAC measurements.

We can do little more than speculate on the B-site structure. It is nonaxial and could be a complex with one vacancy in a first- and one in a second-neighbor position. In view of the large lattice relaxation that we hypothesize, we have made no attempt to compute field gradients for possible B complex arrangements.

Although the exact local structures of the B and C complexes remain to be established definitively, there is no question that C must be a double-vacancy complex, and B must have at least two vacancies. We are surprised that indium forms such strongly bound complexes with two vacancies. We speculate that the small size of the indium atom permits a much stronger local lattice relaxation than occurs for larger dopants and that this relaxation is responsible for both the very strong single-vacancy and the multiple-vacancy binding energies.

The mass action law requires that the relative A-, B-, and C-site occupancies depend on the concentration c_{fv} of free vacancies, and possibly on the conduction electron density c_{fe} if electrons are trapped by any of these centers. Reactions between free vacancies and yttrium atoms or, for pumped samples, between free vacancies and conduction electrons, will generally result in c_{fv} and c_{fe} becoming independent of c when c is large. Therefore, the saturation of the site fractions shown in Fig. 8 at large c is not surprising. Unfortunately, the site-fraction experimental uncertainty at other temperatures precludes reliable estimates of their temperature dependence. These uncertainties arise from complications associated with aftereffects at low temperature and the time dependence of the EFG at high temperature.

D. Site D

The D site is found at a level of 5–25 % in samples doped with sufficient Nb to eliminate oxygen vacancies. The D-site fraction is sample dependent, leading to the inference that it is a complex of indium with an unintentional impurity. The D-site fraction decreases with increasing Nb concentrations. It decreases with temperature, but the site is observed up to nearly 800°C. The EFG is static at all temperatures. We showed that the D site is eliminated if the sample is depleted of oxygen by high-temperature annealing, but the site returns when the sample is annealed in air at 300°C. This observation implies that the bound impurity is mobile at 300°C.

Attempts to remove or deliberately introduce hydrogen failed to change the D-site population, so it seems unlikely that the unknown impurity is hydrogen. We suspect that site D is a complex of indium with an intersti-

tial cation but have made no further attempt to identify it.

E. Aftereffects

Near and below room temperature some of the PAC probe nuclei in all samples are affected by interaction with a metastable trapped electronic defect (which we shall for brevity refer to as a hole, although it may, in principle, be a more complex defect) created in the ^{111}In to ^{111}Cd decay process. The perturbation function due to interaction with these holes decays with time and can be approximated heuristically by the exponential form[12]

$$G_2^a(t) = e^{-\lambda_a t} . \quad (6)$$

We have referred to nuclei subject to this kind of interaction as being in a site X. The expression provides an adequate fit for all spectra except for the uncomplexed probe nuclei of Nb-doped samples. For the latter, the hole escape rate r is apparently comparable to the PAC time scale. For the special case of nuclei in cubic sites, it is possible to include the effect of this escape. Details are given in the Appendix.

The fitted parameters λ_a and r for Nb-doped sample spectra are shown in Fig. 10. We are cautious about the physical interpretation of these parameters. It is not clear why λ_a should be temperature dependent and r should be large for uncomplexed Cd atoms but apparently not for Cd with nearby oxygen vacancies. It is possible that r is large for Nb-doped samples because of hole recombination with conduction electrons, but more work is required to test that hypothesis.

For all other kinds of samples, a substantial fraction of the probe atoms are subject to aftereffects at low temperature, but a sizable fraction clearly do not trap these holes even at 77 K. We analyze these spectra as superpositions of nuclei in sites A, X, and when appropriate, B and C. Equation (6) is assumed to describe site X, and the fit to experimental data is good. λ_a is found to be approximately 200×10^6 s^{-1}. Within experimental uncertainty, no sample or temperature dependence is found.

It is puzzling that some but not all Cd nuclei in samples with nonzero oxygen-vacancy concentration are subject to aftereffects. It is possible that some complex other than the A, B, C, D, or uncomplexed site becomes stable below 150°C but that it is strongly affected by aftereffects, so its "bare" EFG interaction cannot be detected. A second possibility is that probe atoms in the A and B complexes have only approximately 50% probability of trapping a hole after the radioactive decay. Normally, the trapping probability is found to be 100%, but we know of no physical reason to expect this always to be the case. A similar hypothesis of partial trapping has been proposed to explain low-temperature anomalies in ^{181}Hf PAC of zirconium oxide.[17]

Recent calculations by Grimes and Catlow[18] lead us to speculate that the first explanation is the correct one. They find that the trap energy of vacancies trapped by indium is approximately 0.4 eV in either a first- or second-neighbor position. For Cd, they find that vacancies are much more strongly trapped in the first-neighbor position. We speculate the following.

(i) There are roughly equal numbers of first- and second-neighbor vacancies trapped by indium, and there may be double-vacancy complexes other than B and C.

(ii) After ^{111}In decays to ^{111}Cd, single second-neighbor vacancies will eventually move into the first-neighbor position. If that transition rate is of order 10^9/s, then only the first-neighbor PAC spectrum will be found.

(iii) A (electrically neutral) first-neighbor Cd-vacancy complex traps a hole only weakly, but a Cd without a first-neighbor vacancy traps the hole strongly.

The observation of roughly equal fractions of A- and X-sites in undoped low-T ceria follows from the first and third hypothesis. The disappearance of X sites above 150°C follows from the first two hypotheses, provided that the energy barrier between the second- and first-neighbor Cd traps is about 0.4–0.5 eV.

The uncertain origin of the X site greatly complicates analysis of the defect thermodynamics. Such uncertainties do not affect the conclusions of this paper however. We have confined discussion in all other subsections to temperatures above 150°C where no X site is found.

VI. CONCLUSIONS

We find that very dilute indium atoms in cerium oxide trap oxygen vacancies strongly. Unless the concentration of these vacancies is reduced to a negligible level by doping with a pentavalent impurity, indium always traps at least one vacancy, probably at a first-neighbor position. The binding energy of single vacancies to indium is at least 0.35 eV whereas the binding energy of vacancies to most other trivalent dopants is about 0.1–0.3 eV. The trivalent indium ion is smaller than most other trivalent ions, and we speculate that lattice relaxation around the small ion is responsible for the large binding energy. We note that trivalent scandium is even smaller than indium and that scandium-vacancy pairs also have very large binding energy.[1]

The A site is probably a first-neighbor complex of an oxygen vacancy with the ^{111}Cd daughter of the ^{111}In PAC probe atom. At elevated temperature, the bound oxygen vacancy hops among equivalent trap sites around the Cd atom over a barrier height of 0.60(2) eV. The barrier height is equal to the free vacancy barrier deduced from ionic conductivity.

When the oxygen-vacancy concentration is increased to 0.05% or more by doping with yttrium or by vacuum annealing at high temperature, indium also forms complexes with two or more oxygen vacancies. The PAC data indicate that vacancies can hop among trap sites in these multiple-vacancy complexes. The hopping barrier is about 0.6 eV, but the microscopic details cannot be determined from these data.

We find that our cerium samples must be doped with at least 300 ppm Nb/(formula wt.) to remove all oxygen vacancies. The implication is that undoped ceria has an oxygen-vacancy concentration of approximately 75 ppm. It is possible that these are introduced by aluminum im-

purities accidentally incorporated into our samples during processing.

ACKNOWLEDGMENTS

This research was supported in part by the U.S. Department of Energy Grant No. DE-FG06-85ER45191. We appreciate technical assistance from R. Lundquist and M. Preddy.

APPENDIX

1. Data analysis

During a PAC measurement, the spectrometer computer collects histograms $D_{\alpha\beta}(t)$ of events for which the first γ ray enters detector α and the second enters detector β at time t later. 512 channels of width 2 ns were accumulated for each α-β combination. The stop time pulse is delayed so the time = 0 channel, t_0, is near the middle of the histogram. This is required with our spectrometer design[8] so that 8 α-β combinations (the 180° pairs 0-2, 2-0, 1-3, 3-1, and the 90° pairs 1-2, 2-1, 0-3, and 3-0) can be accumulated. The spectrometer time resolution is smaller than the channel width.

The random count rate for each α-β pair is the average of the counts/channel at large positive and negative times. This random rate is subtracted to obtain the real count rate $c_{\alpha\beta}(t)$. Two statistically independent experimental time functions were formed,

$$[A_2G_2(t)]_0 = \frac{2[c_{02}(t)c_{13}(t) - c_{12}(t)c_{03}(t)]}{[c_{02}(t)c_{13}(t) + 2c_{12}(t)c_{03}(t)]} \quad \text{(A1)}$$

and

$$[A_2G_2(t)]_1 = \frac{2[c_{20}(t)c_{31}(t) - c_{21}(t)c_{30}(t)]}{[c_{20}(t)c_{31}(t) + 2c_{21}(t)c_{30}(t)]} \quad \text{(A2)}$$

for each time channel. Each time function was fitted independently, and within experimental uncertainties, the fitting parameters were the same for each function. Fitting parameters shown in this paper are the mean of the two independent fits.

Data were fitted between time channel $t_0 + 2$ and the time at which the statistical errors become large—typically the time at which the real and random count rates are comparable. The minimum time channel was chosen at 2 past t_0 to eliminate artifacts associated with the shape of the histogram at t_0. For all fits except those in which the fraction f_X of nuclei subject to the aftereffects interaction is large, the fitted parameters are insensitive to the choice of starting channel. In particular, the anisotropy A_2 agrees well with calibrated values, an indication that no important effects are masked by neglecting data in channels t_0 and $t_0 + 1$.

The only fitting parameters that are affected by choice of starting channel are the fraction f_X and decay rate λ_a of the function $G_2^a(t)$ given by Eq. (6) which we use to model the PAC time function of nuclei subject to "after-effects" interactions. We do not know how to model this interaction rigorously. Equation (6) is a heuristic choice that provides an adequate fit, although it is clearly not rigorously correct.

For all samples except those doped with more than 400 ppm Nb or Ta, data taken below 300°C show unambiguously that a substantial fraction of the ^{111}Cd nuclei are subject to one or more electric field gradient interactions. Below 150°C, $G_2(t)$ displays a substantial decay near the origin. The decay is characteristic of aftereffect interactions with metastable electronic configurations caused by the ^{111}In electron capture decay which we model by Eq. (6). For these materials, all data below 150°C were fitted using the perturbation function

$$G_2(t) = f_X G_2^a(t) + \sum_{n=A,B,C} f_n G_2^n(t), \quad \text{(A3)}$$

where $G_2^n(t)$ is the perturbation function for a static EFG interaction at site n, given by Eq. (1), and f_n are the fractions of nuclei in site n.

We note that it is also necessary to account for a small contribution, approximately -0.007 for all $A_2G_2(t)$ data. This shift is an experimental artifact caused by γ ray absorption in the sample.[19] It is a function of sample diameter and density, and cannot easily be reduced without using sample diameters that are experimentally impractical. The exact magnitude of the shift is not critical; ignoring it entirely would introduce only minor errors in fitting parameters.[20]

For undoped, lightly Nb-doped, lightly Y-doped, and all In-doped ceria samples that have not been deliberately made oxygen deficient, only site A is included in the computer fits. For more heavily Y-doped samples and for oxygen-deficient samples, sites B and C must be included. In general, the anisotropy A_2, the aftereffects parameters f_X and λ_a, the interaction frequencies, ω_1 and ω_2, for each site, and the site fractions f_n are fitted. The sum of the site fractions is forced to unity, and ω_3 is set equal to $\omega_1 + \omega_2$. The fitted parameters are shown in Figs. 4 and 8.

Above 150°C for these materials, f_X becomes negligible. Between 150 and 300°C, there is still clearly an EFG interaction, but the oscillations are noticeably damped, and the frequencies decrease substantially with temperature as T approaches 300°C. These qualitative features indicate that the EFG is no longer static. Physical intuition suggests that the EFG arises from an associated defect complex and that the time dependence must arise either from detrapping or reorientation of the defect. Detrapping of a defect is considered in the second subsection of the Appendix, and the expression does not describe the experimental data. If we assume that the time dependence is due to reorientation of the complex, then the XYZ model considered by Evenson *et al.*[11] should be applicable. The assumptions of this model are that a given nucleus can be subject to an EFG whose principal axis elements are constant but whose directions can assume one of several orientations. It is assumed that the EFG changes stochastically among the possible orientations at rate w and that the time average of the EFG is

zero. These assumptions are reasonable for most types of reorienting defect complexes in ceria. The XYZ model is the simplest case, for which the EFG is axially symmetric with three mutually orthogonal directions allowed for the Z principal axis. When w is sufficiently small, the XYZ model perturbation function $G_2^{XYZ}(t)$ is the static $G_2(t)$ appropriate for that EFG. For larger w, the interaction becomes damped in time, and the apparent interaction frequencies go continuously to zero at some w. For larger w, $G_2^{XYZ}(t)$ is a sum of decaying exponentials, $\exp(-\lambda_k t)$, whose λ_k coefficients are monotonically decreasing functions of w. For sufficiently large w, $G_2^{XYZ}(t)$ cannot be distinguished experimentally from unity.

Evenson *et al.* argue that the XYZ perturbation function is semiquantitatively applicable to cases where the EFG can assume more than three orientations, although the rate, w, may not be correctly normalized. They also suggest a heuristic method for application to nonaxial EFG interactions.

For samples having only the A site near 200°C, we have fitted all data with the XYZ model. At lower temperature, all parameters could be fitted, and the EFG was found to be negligibly temperature dependent. At higher temperature, the EFG was fixed at its low-T value. All fits were excellent. Figure 5 shows that w follows an activated behavior with temperature and has no discontinuity at 300°C where the experimental time function changes character qualitatively.

The temperature-dependent characteristics of the B and C sites are similar to the A site. The C-site intensity is too small to make meaningful fits, but we have fitted the B site to the XYZ model and find the w values shown in Fig. 5. For these fits the A site parameters were fixed and the C site was assumed static at low T and only crudely approximated at higher temperature. Because of its smaller intensity and these approximations, the B-site fluctuation rate w is not as accurately determined as that of the A site.

For samples doped with more than 400 ppm Nb or Ta, a small fraction, typically 5–25 % of the PAC probe nuclei were subject to a static interaction we have called site D. The majority were apparently in uncomplexed sites subject to no EFG but which were subject to aftereffects at lower temperatures. A standard static interaction [described by Eq. (1)] is assumed for the D site, and Eq. (A3) is assumed to describe nuclei in uncomplexed sites. The D-site frequencies are shown in Fig. 4, and the parameters λ_a and r for the aftereffected, uncomplexed site are shown in Fig. 10.

2. PAC time function due to a metastably trapped defect in a cubic host

The PAC time function for nuclei interacting with a trapped defect may usually be represented by a sum of damped cosines,

$$G_2^d(t) = \sum_j S_j e^{-\lambda_j t} \cos \omega_j t \ . \tag{A4}$$

If the defect is trapped at $t = 0$ but has a detrapping rate r large enough that detrapping on the time scale of $G_2(t)$ is not negligible, then the measured time function may not be well represented by Eq. (A4). In the special case where the host is cubic, we can derive a general expression for the PAC time function, $G_2(t)$, as a function of r and the parameters of $G_2^d(t)$. This is possible because there is no perturbation following detrapping, and the contribution of any nucleus to $G_2(t)$ remains constant after the defect has detrapped. We note that the fraction of nuclei with trapped defects at any time t is $p(t) = \exp(-rt)$, so that

$$G_2(t) = G_2^d(t)e^{-rt} + \int_0^t G_2^d(t')e^{-rt'} r \, dt' \ . \tag{A5}$$

The first term is the contribution to the time function from nuclei that still have trapped defects at time t, and the latter term is due to nuclei whose contribution was G_2^d until the defect detrapped at time $t' < t$. Combining Eqs. (A4) and (A5), we obtain

$$G_2(t) = \sum_j S_j \left[a_j + e^{-(r+\lambda_j)t} \left(b_j \cos \omega_j t + c_j \sin \omega_j t \right) \right] \ , \tag{A6}$$

where

$$a_j = \frac{r(r+\lambda_j)}{\omega_j^2 + (r+\lambda_j)^2} \ ,$$

$$b_j = 1 - \frac{r(r+\lambda_j)}{\omega_j^2 + (r+\lambda_j)^2} \ ,$$

$$c_j = \frac{r\omega_j}{\omega_j^2 + (r+\lambda_j)^2} \ .$$

Such an expression should be applicable for aftereffects in cubic materials and for cases where an interstitial impurity or lattice defect trapped by the parent detraps quickly after the electron capture decay. For the special case of Eq. (6) where $G_2^d(t)$ consists of a single damped exponential, the above relation reduces to[13,20]

$$G_2(t) = \frac{r}{r+\lambda} + \frac{\lambda}{r+\lambda} e^{-(r+\lambda)t} \ . \tag{A7}$$

[1] A. S. Nowick, *Diffusion in Crystalline Solids* (Academic, New York, 1984).

[2] *Proceedings of the First International Conference on the Science and Technology of Zirconia*, edited by A. H. Heuer and L. W. Hobbs (American Ceramic Society, Columbus, OH, 1981).

[3] R. Wang, J. A. Gardner, W. E. Evenson, and J. A. Sommers, *Point Defects and Related Properties of Ceramics*,

Ceramic Transactions Vol. 24, edited by T. O. Mason and J. L. Loutbort (American Ceramic Society, Westerville, OH, 1991).
[4]J. A. Gardner, H. Jaeger, H. T. Su, and J. C. Haygarth, Physica B **150**, 223 (1988).
[5]H.-T. Su, R. Wang, H. Fuchs, J. A. Gardner, W. E. Evenson, and J. A. Sommers, J. Am. Ceram. Soc. **73**, 3215 (1990).
[6]H.-T. Su, Ph.D. thesis, Oregon State University, 1989 (unpublished).
[7]D. Y. Wang, D. S. Park, J. Griffith, and A. S. Nowick, Solid State Ionics **2**, 95 (1981).
[8]H. Jaeger, J. A. Gardner, H. T. Su, and R. L. Rasera, Rev. Sci. Instrum. **58**, 1694 (1987).
[9]H. Frauenfelder and R. M. Steffen, in *Alpha-, Beta-, and Gamma-Ray Spectroscopy*, edited by K. Siegbahn (North-Holland, Amsterdam, 1965), Vol. II.
[10]W. E. Evenson, A. G. McKale, H. T. Su, and J. A. Gardner, Hyperfine Interact. **61**, 1379 (1990).
[11]W. E. Evenson, J. A. Gardner, R. Wang, H.-T. Su, and A. G. McKale, Hyperfine Interact. **62**, 283 (1991).
[12]U. Baeverstam, R. Othaz, N. deSousa, and B. Ringstrem, Nucl. Phys. A **186**, 500 (1972).
[13]A. G. Bibiloni, C. P. Massolo, J. Desimoni, L. A. Mendoza-Zélis, F. H. Sánchez, A. F. Pasquevich, L. Damonte, and A. R. López-García, Phys. Rev. B **32**, 2393 (1985).
[14]R. N. Blumenthal, J. Solid State Chem. **12**, 307 (1975).
[15]H. L. Tuller and A. S. Nowick, J. Phys. Chem. Solids **38**, 859 (1977).
[16]H. L. Tuller and A. S. Nowick, J. Electrochem. Soc. **126**, 209 (1979).
[17]H. Jaeger, H. T. Su, J. A. Gardner, I.-W. Chen, J. C. Haygarth, J. A. Sommers, and R. L. Rasera, Hyperfine Interact. **60**, 615 (1990).
[18]R. Grimes and C. R. A. Catlow (private communication).
[19]P. C. Lopiparo and R. L. Rasera, in *Angular Correlations in Nuclear Disintegrations*, edited by E. van Krugten and B. van Nooijen (Rotterdam University Press, Rotterdam, 1971), p. 66.
[20]R. Wang, Ph.D. thesis, Oregon State University, 1991 (unpublished).